Observations of the Shelf-Edge Current South of Australia, Winter 1982

J. S. GODFREY AND D. J. VAUDREY

CSIRO Division of Oceanography, Hobart, Tasmania, 7001

S. D. HAHN

Flinders Institute for Atmospheric and Marine Sciences, Flinders University, Bedford Park, South Australia, 5042

(Manuscript received 23 April 1985, in final form 15 July 1985)

ABSTRACT

Results are presented from an oceanographic cruise along Australia's south coast in June–July 1982. A narrow shelf-edge current flowed eastwards along the shelf edge for the entire distance. Features of particular interest were (i) various eddies on the offshore side of the current, (ii) very sharp surface fronts, at which geostrophic Richardson numbers were less than 1.0 in 10 out of 34 cases, (iii) the formation and offshore transport of saline water in the Great Australian Bight, and (iv) the strongly nonlinear dynamics in the neighborhood of Cape Leeuwin.

1. Introduction

This paper describes the results from an oceanographic cruise (SP6/82) by R/V *Sprightly* from Fremantle, Western Australia to Portland, Victoria between 18 June and 4 July 1982 (Figs. 1–3). The region is of considerable interest oceanographically: Cresswell and Golding (1980) have demonstrated the existence of a strong, narrow current (the Leeuwin Current) along the continental shelf edge, from about 22°S off the Western Australian coast, around Cape Leeuwin and into the Great Australian Bight. It is strongest in (southern) autumn and winter; current speeds of 1.5 m s^{-1} sometimes occur near Cape Leeuwin. Rochford (1985) showed, from a cruise in June 1971, that the shelf-edge currents were strongly baroclinic, with isotherms sinking from the surface to as much as 200 m below the surface, over distances less than the station spacing of about 40 km. Satellite infrared images show that the surface fronts separating relatively warm shelf water from cold ocean water are very sharp, (e.g., Legeckis and Cresswell, 1981; Pearce, personal communication, 1984), while winter current meter records show currents of up to 0.5 m s^{-1} inshore from these shelf-edge fronts in the eastern Great Australian Bight (Provis and Lennon, 1981). The satellite images also often show "tufts" or "modons" of warm water breaking away from the shelf and curling back towards the west, possibly associated with the cyclonic eddies that occur on the offshore edge of the current (Cresswell and Golding, 1980; Griffiths and Pearce, 1985). Further features of interest are the temperature inversions observed near the 200 m isobath south of Kangaroo Island; Kitani (1977) suggests that these are associated with the sinking of saline water from the inner continental shelf of the Great Australian Bight and Spencer's Gulf.

The cruise reported here was the first major physical oceanographic survey of the south coast of Australia since these discoveries were made.

Section 2 deals with the methods of observation used. Sections 3–8 deal with various aspects of the results, and these are discussed in Section 9. Since the paper deals with a number of different physical phenomena, a summary of our results is given in Section 10.

2. Methods

Figures 1a, 2 and 3a show the cruise track, and the 200 m isobath. The continental shelf edge is very sharply defined along the entire track, with the 150 and 500 m isobaths (not shown) seldom more than 20 km apart; the track was basically a series of oblique crossings of the continental slope, with a few excursions to the shelf and the deep ocean. One hundred seventeen hydrographic stations were taken to within 10 m of the bottom or to 1000 m, using a Neil Brown Mark III CTD. Temperature, salinity, dissolved oxygen, inorganic phosphate, silicate and nitrate were measured at up to 12 depths on each cast, using a rosette sampler. Expendable bathythermographs, 103 in all, were also dropped giving profiles of temperature to 450 m accurate to ±0.2°C. A surface thermosalinograph provided a continuous record of temperature at about 10 m depth (accurate to ±0.2°C) and salinity (to ±0.05%).

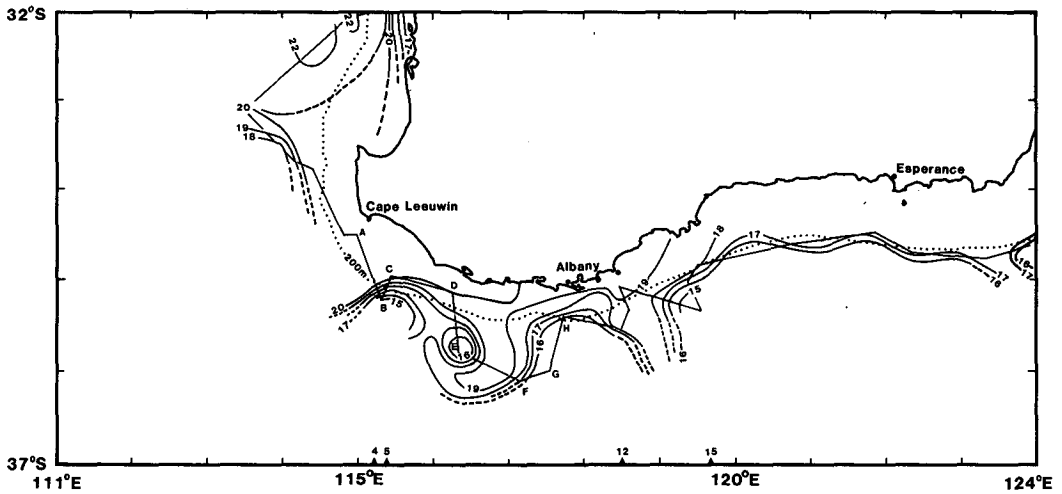

FIG. 1a. Cruise track (light line) and surface isotherms in °C (heavy lines) from 111°E to 124°E, 18–24 June 1982. Numbered arrowheads along the borders point to fronts whose along-track Richardson numbers were less than one (see Table 1). The 200 m isobath is shown as a dotted line. The vertical sections of Fig. 9 were taken along AB, BC, DEF, and FGH.

Four satellite-tracked buoys, each drogued to 20 m, were released; their tracks are shown in Figs. 1–3. They reported sea surface temperature (SST) which has been used in the first few days of each buoy track to supplement SSTs from the surface thermosalinograph. Although some satellite infrared photographs of the region were obtained on 11, 28 and 30 June 1982 (Pearce, private communication, 1984), cloud covered much of the region, particularly in the west. However, winds were light during most of the cruise, so ship's drift vectors provided a useful qualitative guide to the currents in the region.

3. Surface isotherms, ship's drift vectors and buoy tracks

Figures 1a, 2 and 3a show surface isotherms in the western, central and eastern sections of the cruise track. Satellite infrared images of the region show that SST patterns are often rather complex, so that the accuracy of these SST maps must decrease rapidly away from the ship's track, except in those parts of Figs. 1–3 where cloud-free satellite infrared images were available within 10 days before or after the cruise. (This occurred between 119°E and 130°E.) Near fronts, isotherms in

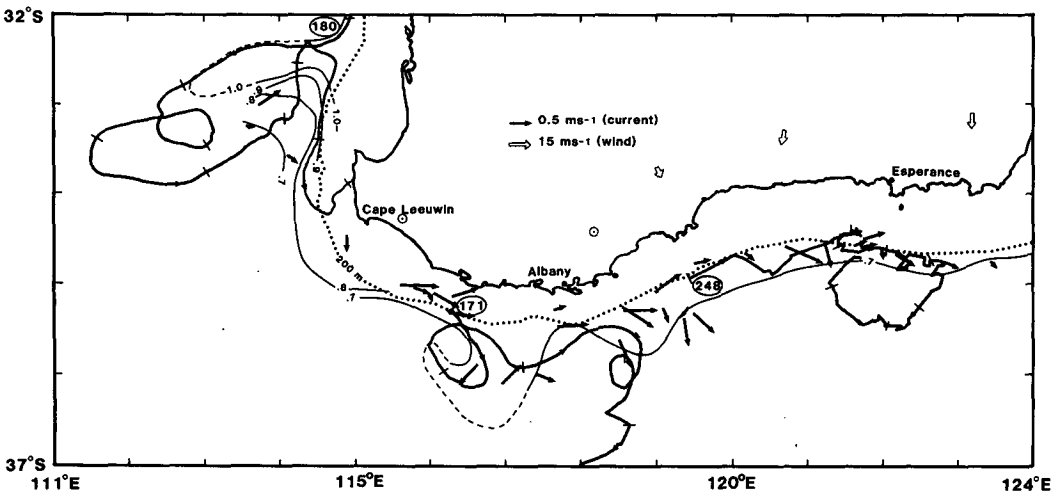

FIG. 1b. Steric height relative to 450 db (light lines, contour values in m), ship's drift vectors (arrows) and buoy tracks (heavy barred lines) from 111°E to 124°E, 18–24 June 1982. Bars are shown along buoy tracks every 3 days. Day numbers in 1982 are shown inside ellipses at the start of each track; the track starting near (34°45′S, 119°50′E) is the continuation of the track starting near (35°23′S, 116°22′E). Wind vectors encountered along the track are also shown, over land to the north of the point where they were encountered.

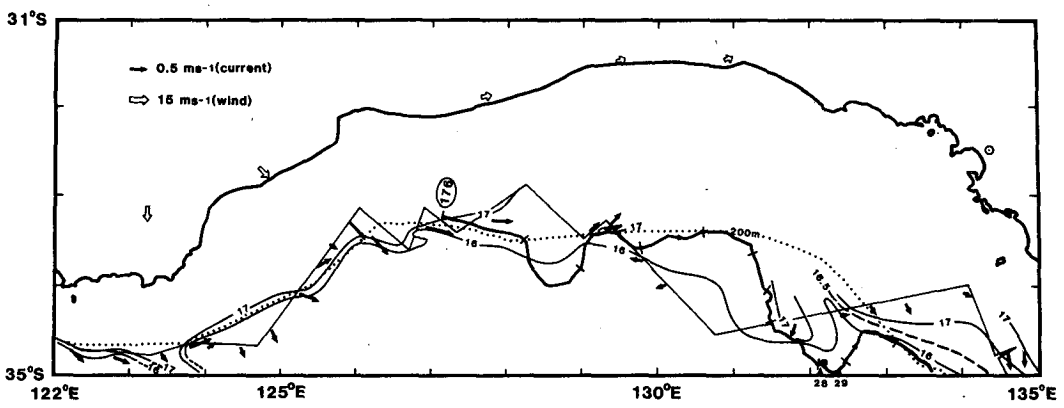

FIG. 2. Cruise track (light line), ship's drift vectors (arrows), SST contours (heavy lines) and buoy tracks (heavy lines, with bars every 3 days), and wind vectors (arrows over land), from 122° to 135°E, 23–28 June 1982. Numbered arrows along the southern border point to fronts whose along-track geostrophic Richardson numbers are less than one (see Table 1). The 200 m isobath is shown as a dotted line.

Figs. 1a, 2 and 3a were drawn parallel to the ship's drift vectors obtained on either side of the front, and SSTs from satellite-tracked buoys were also used in the first few days after release. The buoy tracks themselves (Figs. 1b, 2, 3b) were not used in drawing these isotherm maps. The buoy tracks reflect the SST features fairly accurately, even when several tens of days separate the buoy tracks from the SST observations; thus buoy tracks in Fig. 1b show cyclonic loops centered near 116°20′E, 118°30′E and 122°E. These loops occurred about 3, 10 and 90 days respectively, after the SST observations of Fig. 1a were made. All three loops occur just to the west of "tufts" of warm water emanating from the shelf. Further east buoy tracks leave the continental shelf seawards in a series of anticyclonic arcs (at 128°–129°E, 131°–133°E, and perhaps also at 137°–138°E) rather than forming cyclonic loops. At 132° and 137°E these arcs are associated with tongues of warm surface water that move offshore at a shallow angle to the continental shelf. South of Kangaroo Island (Fig. 3b), the buoy track shows a small, complex pair of loops across the continental shelf edge; a second buoy track (not shown) entered the same region 50 days later, and experienced a similar complex, small-scale diversion from its generally southeastward flow. Some of these features will be discussed later in the paper.

4. Steric sea levels

Contours of steric sea level relative to 450 db (Figs. 1b, 3b) indicate a flow pattern in broad agreement with that from buoy tracks and ship's drift vectors. Figure 4a shows the steric sea level relative to 450 db, as a

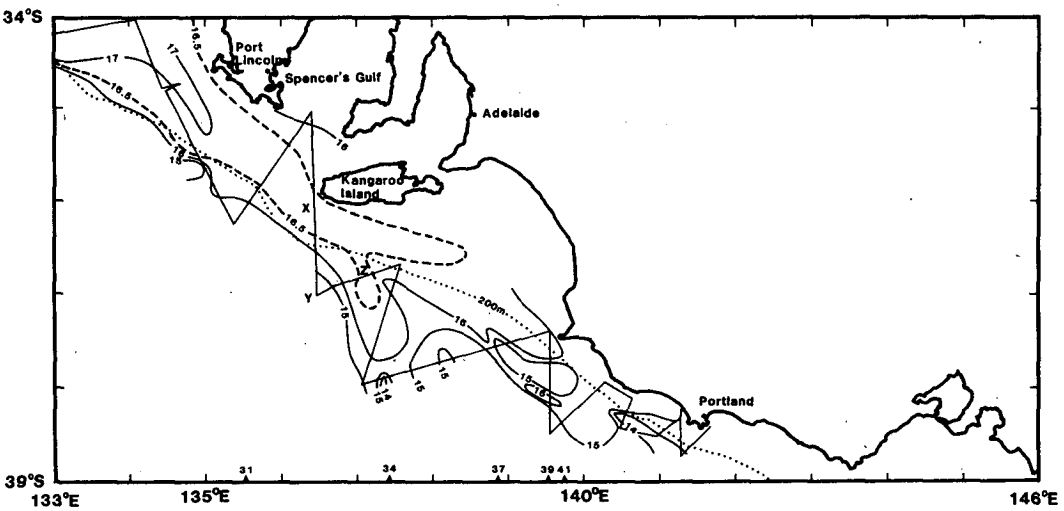

FIG. 3a. As in Fig. 1a but for 133°–146°E, 27 June–4 July 1982.
The vertical salinity section of Fig. 11 is taken along XY.

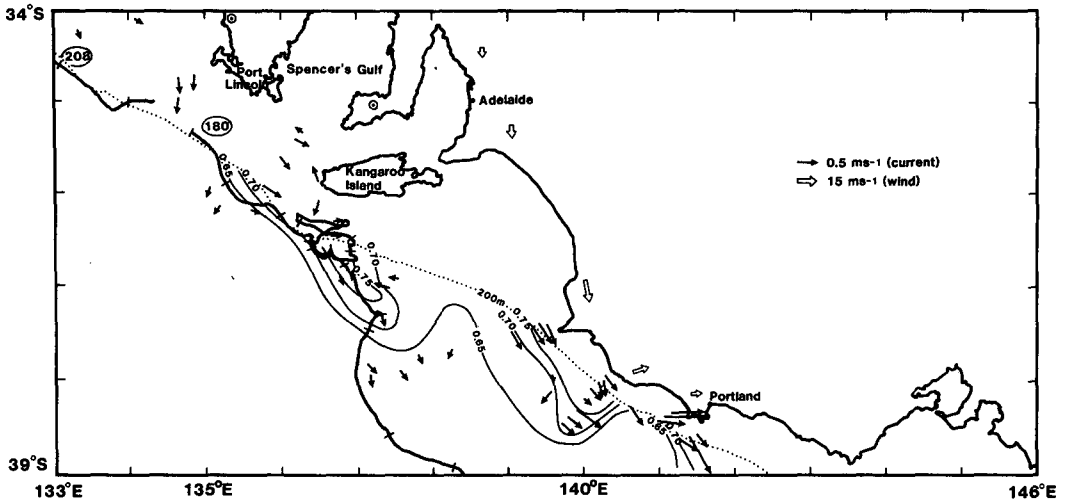

FIG. 3b. As in Fig. 1b but for 133°–146°E, 27 June–4 July 1982.

function of latitude (north of Cape Leeuwin) and longitude (east of Cape Leeuwin): the dashed curve shows all values obtained at offshore corners of the cruise track of Figs. 1–3 (all more than 30 km offshore from the 500 m isobath), while the full curve shows all values obtained near the 500 m isobath. The inshore sea level is greater than the offshore sea level, except near 138°E; this discrepancy is associated with the Kangaroo Island eddy (Fig. 3b). While our sampling was sparse, this seems to imply a continuous eastward current everywhere along the southern Australian shelf edge. This idea is also supported by the fact that a tropical coccolithophorid (*Scyphosphaera apsteinii*) was present in a continuous sample series taken during this and a subsequent cruise from Cape Leeuwin to Western Tasmania (G. Hallegraeff, personal communication, 1984).

The inshore–offshore steric height difference relative to 450 db, and therefore the longshore current, appears to be weak over the Great Australian Bight. However, this may be misleading: the current may be present, but inshore from the 500 m isobath. This can be seen in Fig. 4b, which shows inshore and offshore curves for steric sea level relative to 200 db; the offshore (dashed) curve is obtained from the same stations as

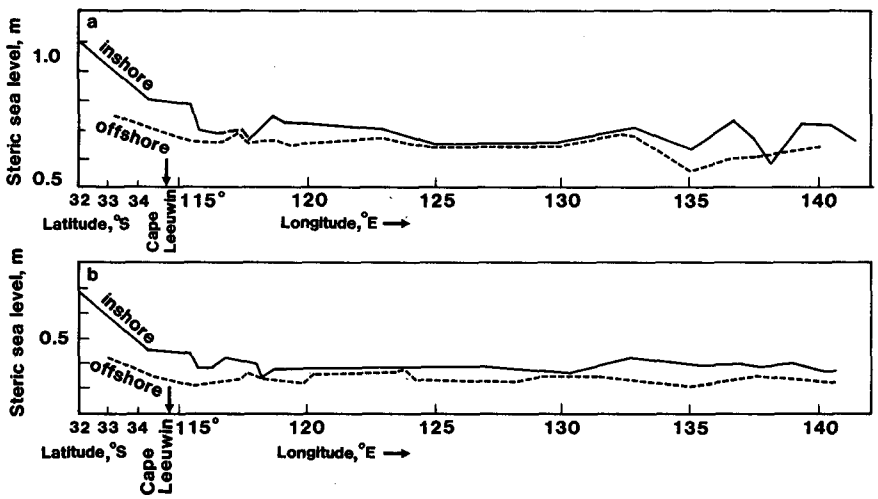

FIG. 4a. Steric sea level relative to 450 db, at inshore and offshore stations, plotted as a function of latitude (Fremantle to Cape Leeuwin) and longitude (east of Cape Leeuwin). "Offshore" stations occur at the offshore corners of the cruise track, all 30 km or more offshore from the 500 m isobath; "onshore" stations occur near the 500 m isobath.

FIG. 4b. As in Fig. 4a, but steric sea level relative to 200 db is shown, and the nearshore stations occur near the 200 m isobath.

Fig. 4a, but the "inshore" curve comes from stations near the 200 m isobath. It may be seen in Fig. 4b that the difference between inshore and offshore steric sea levels is rather a smoother function of longshore distance than that for steric height relative to 450 db.

A feature of particular interest is the steric sea level drop (relative to 450 db) of 0.21 m along the 500 m isobath, from Fremantle to west of Cape Leeuwin; there is a further sharp drop of 0.1 m across the oblique front south of Cape Leeuwin, for a total of 0.3 m in 400 km in the longshelf direction. Large scale maps show a steric sea level drop (relative to deeper reference levels) of about 0.55 m along the Western Australian continental shelf from 22°S to 34°S, i.e., over a distance of about 1400 km. Thompson (1984) and Godfrey and Ridgway (1985) suggested that this unusually large steric sea level gradient was not in accurate geostrophic balance near the continental shelf edge, and that it is primarily responsible for accelerating the Leeuwin Current. Our observations suggest that at the time of our cruise, most of this steric sea level drop occurred over the 400 km from Fremantle around Cape Leeuwin.

However, Fig. 4 shows the steric sea level gradient to be near zero, east of 118°E. Presumably the observed longshelf currents are driven by the prevailing westerly winds in this region, or by independent thermohaline effects associated with different cooling rates on and off the continental shelf, or by a combination of both.

5. Water mass properties

The dots in Fig. 5 show the temperature–salinity values for ten stations at offshore corners of the cruise track of Figs. 1–3. A tightly defined T–S relationship can be seen passing through the dots (full line); thus the offshore water appeared to form a single water mass over the entire length of the cruise. The values between 5° and 17.5°C are consistent with Ridgway and Loch's (1985) T–S curves for the region.

On the continental shelf west of 127°E, T–S values are loosely scattered about the high-temperature end of the offshore T–S curve (diamonds in Fig. 5). However, on the shelf east of 127°E (black squares, Fig. 5) much higher salinities were found, due presumably to the strong evaporation in the Great Australian Bight. The highest salinities of 36.2‰ or greater were found inside Spencer's Gulf, with temperatures of about 15°C. However, water with salinity of over 36.0‰ was found at several stations near (34°S, 134°E), with temperatures between 16° and 17°C.

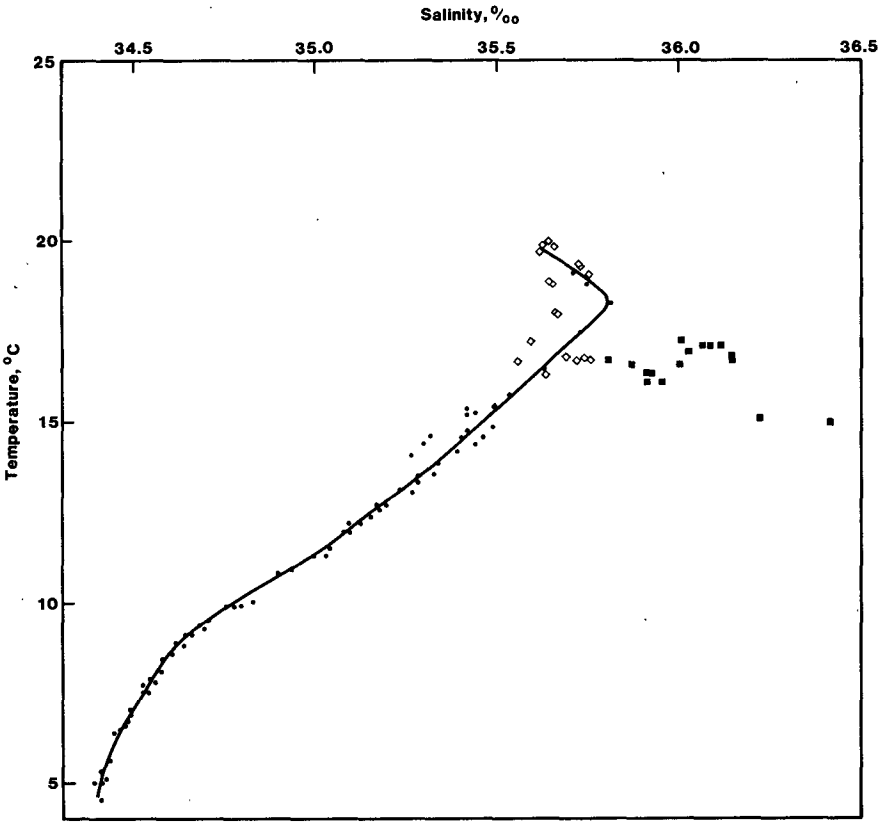

FIG. 5. Temperature–salinity results for the cruise. The dots represent T–S values at 10 stations at offshore corners of the cruise track, offshore from the 1000 m depth contour, diamonds and squares represent T–S values obtained on the shelf, west and east, respectively, of 127°E.

Near 137°E, an extensive tongue of high-salinity water was found at around 200 m depth beyond the shelf edge; from its temperature of over 16°C, it seems clear that this tongue originated primarily from the eastern Great Australian Bight source, rather than from Spencer's Gulf. Further details of this and other shelf-edge high-salinity layers are given in Section 8.

Plots of oxygen against temperature and of phosphate against temperature were not as well-defined as the temperature–salinity plot of Fig. 5, and they revealed little new information that could be used for water mass tracing. The only exception was that the westernmost deep stations contained a layer of highly oxygenated (5.8 ml l^{-1}) water at temperatures of 9°–10°C, not found in stations east of Cape Leeuwin.

6. Surface fronts and geostrophic Richardson numbers

Satellite images show that near a given longitude, surface temperature along Australia's south coast typically has one well-defined maximum value T_{max} just inshore from the continental shelf edge, and a second fairly well-defined value T_{min} between eddy features offshore from the shelf edge (e.g. Fig. 6). The difference $(T_{max} - T_{min})$ decreases from about 5°C near Cape Leeuwin to 1.5°C near 140°E. In this paper, whenever SST changed by more than half of the subjectively estimated local value of $(T_{max} - T_{min})$ in a distance of 30 km or less along the ship's track, it has been treated as a front; 45 fronts satisfying this definition were crossed. Some of them are indicated by arrowheads along the borders of Figs. 1a, 2 and 3a. There was a very strong tendency for well-defined fronts to occur just offshore from the 200 m isobath, particularly west of 136°E; between Cape Leeuwin and 136°E, 15 straight sections of cruise track covered the region from 10 km inshore from the 200 m isobath to 40 km offshore from it and on every one of these sections a "positive" front was found between 5 and 25 km offshore. [A (positive/negative) front has the warm water on the (nearshore/offshore) side]. This pattern tended to break down east of 136°E. Eight sections of the cruise penetrated 75 km seaward of the 200 m contour. On these eight sections, apart from the group of nearshore positive fronts just mentioned, there was a second group of four negative fronts, all lying between 30 and 40 km offshore; beyond that a further group of four positive fronts occurred, all between 40 and 65 km offshore.

It is convenient to define a bulk measure of the sharpness of each front, based on the "geostrophic Richardson number"

$$\mathrm{Ri}_G = \frac{g}{\rho_0}\frac{\partial \rho}{\partial z}\Big/\left(\frac{g}{\rho_0 f}\frac{\partial \rho}{\partial x}\right)^2 \qquad (1)$$

where the denominator is the square of the geostrophic approximation to the vertical velocity shear; ρ is the water density, f the Coriolis parameter, and z, x measure distance vertically and perpendicularly to the front. Across surface fronts such as the two shown in Figs. 6 and 10c, a bulk approximation to Ri_G can be made in the dotted triangular regions PQR, P′Q′R′ of Fig. 10c, namely:

$$\mathrm{Ri}_G = \frac{f^2 \Delta X^2 \sin^2\theta}{(g/\rho_0)\Delta\rho\,\Delta z}. \qquad (2)$$

Here ΔX is the horizontal distance along the ship's track from the SST minimum on the cold side of the front (T_{min}) to the XBT or CTD station in the warm side, shown as ΔX_6 and ΔX_7 for the two fronts in Fig. 6, and $\Delta\rho$ is the difference in surface density between these two points. In (2) θ is the angle between the ship's track and the tangent to the front, and Δz is the depth at which T_{min} is found, on the XBT or CTD on the warm side of the front, (the dashed triangles around fronts in Fig. 10 have base ΔX at the surface, and depth Δz). For all but a few very weak fronts east of 139°E, the offshore T–S relation of Fig. 5 was a good approximation both for the surface T–S values and along vertical profiles, so the horizontal density difference $\Delta\rho$ across the front is also the vertical density difference from the surface to depth Δz, on the warm-side thermal

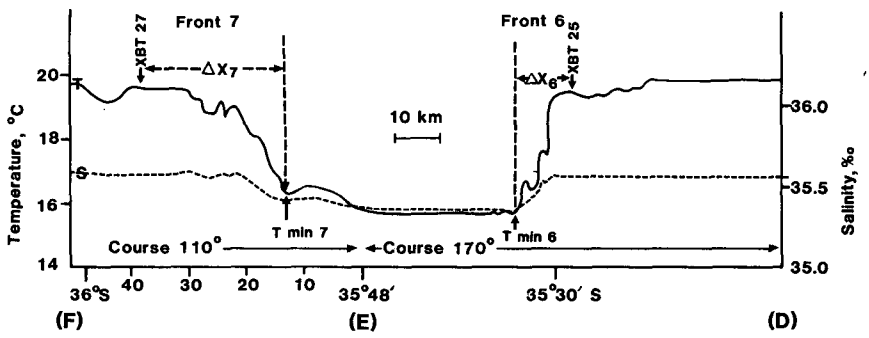

FIG. 6. Surface temperature (full line) and salinity (dashed line) along DEF of Fig. 1a, plotted as a function of along-track distance. Along-track geostrophic Richardson numbers Ri_A are estimated for fronts 6 and 7 using XBTs 25 and 27, dropped near the warm edges of each front. The distances ΔX_6 and ΔX_7 for use in (3) are shown.

profile. In practice, the direction of the front (and therefore the angle θ) was poorly known, except in a few instances; but it may be noted that the "along-track geostrophic Richardson number":

$$\mathrm{Ri}_A = f^2 \Delta X^2 \Big/ \frac{g\Delta\rho}{\rho_0} \Delta z \qquad (3)$$

is an upper limit to the true value of Ri_G. Of the 45 fronts encountered, a measurement of Ri_A was made on 34. (For fronts 6 and 7 of Figs. 6 and 10c, Ri_A was 1.6 and 8 respectively for our choices of $T_{\min}$). A histogram of values of Ri_A from these 34 fronts is shown in Fig. 7. It might be expected that the shelf edge group of fronts, being associated with the main longshore current, might be particularly sharp; however, there was no clear tendency for the nearshore group of fronts to be "sharper" (have lower Ri_A) than those further offshore. A histogram of the depths Δz is shown in Fig. 8: the Δz values are rather sharply grouped around a median value of about 100 m.

Details of ten "sharp" fronts for which Ri_A was less than 1.0 are given in Table 1, and their locations are shown by numbered arrowheads along the borders of Figs. 1a, 2 and 3a.

Frontal regions with such small bulk geostrophic Richardson numbers may contain substantial shear layers with true Richardson numbers less than 1/4; such regions are subject to Kelvin–Helmholtz instability (e.g., Turner, 1973), and turbulent shear stresses will develop across them. Crude order of magnitude estimates (e.g., Godfrey et al., 1980; Hebert and Garrett, personal communication, 1984) suggest that these stresses may be comparable to typical wind stresses (0.1 Pa) or larger. Since they occur in narrow, elongated patches a few kilometers wide along the edges of particularly sharp fronts, the curls of these stresses may be extremely large compared to typical wind stress curls, since the length scales of the latter are typically hundreds or thousands of kilometres.

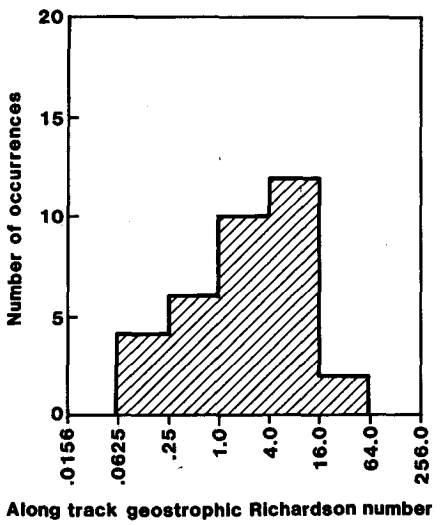

FIG. 7. Histogram of values of along-track Richardson number, for 34 fronts.

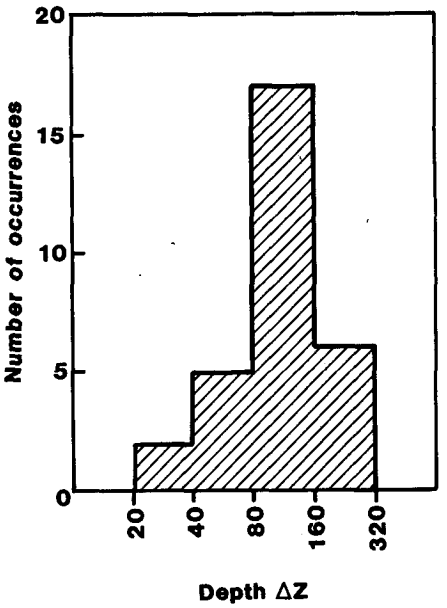

FIG. 8. Histogram of values of Δz, for 34 fronts.

Several small but very sharp density fronts were also found on the continental shelf, east of 127°E; however, the density difference in these fronts was due to salinity alone. Figure 9 shows the thermosalinograph record obtained on the section from (34°40′S, 130°40′E) to (34°S, 134°10′E). A regular and sharp sequence of "steps" can be seen in the surface salinity, with little change in the temperature; these fronts are delicate and shallow, and they are presumably destroyed in any strong wind. Their alternate formation and destruction in calm and windy periods may play a significant role in transferring salty water seaward from the head of the Great Australian Bight. Unfortunately, these in-

TABLE 1. Characteristics of sharp fronts.

Front number	Type (+ or −)	$T_{\min}$ (°C)	ΔT (°C)	$\frac{\Delta\rho}{\rho_0}$ ($\times 10^{-3}$)	ΔX (km)	Δz (m)	Ri_A
4	+	15.0	4.8	1.0	10.0	175	0.39
5	+	16.1	3.3	0.62	2.5	40	0.18
12	+	15.7	2.5	0.62	6.0	115	0.35
15	+	16.7	1.9	0.42	6.0	60	1.0
29	+	15.2	1.5	0.20	3.0	150	0.21
31	+	15.2	1.0	0.15	3.0	75	0.59
34	+	14.0	1.3	0.18	1.5	70	0.13
37	+	14.7	1.3	0.18	4.5	100	0.8
39	−	15.0	1.0	0.15	4.5	155	0.6
41	+	14.6	1.1	0.15	3.0	175	0.24

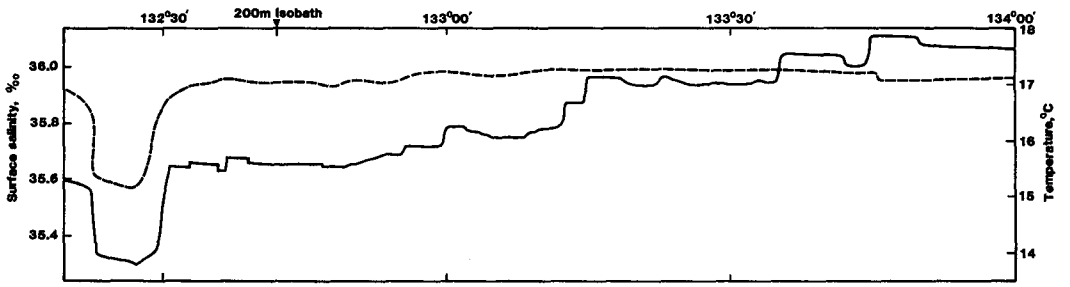

FIG. 9. Surface temperature (dashed line) and salinity (full line) between 34°20'S, 132°20'E and 34°05'S, 134°E.

teresting features are not amenable to study by satellite infrared imagery, since the temperature differences across them are so small.

7. Flow behavior near Cape Leeuwin

Flow speeds near Cape Leeuwin consistently reach values comparable to those in western boundary currents; to our knowledge, there is no other place in the world where this occurs near an oceanic eastern boundary. The flow behavior near Cape Leeuwin is thus of particular dynamical interest.

The buoy tracks are discussed first. Of five previous cases of buoy tracks passing Cape Leeuwin near the continental shelf edge (Cresswell and Vaudrey 1977; Cresswell and Golding 1980), three entered the Leeuwin Current from an offshore eddy, accelerated southwards to speeds of order 1.5 m s^{-1} over a longshore distance of about 100 km, and then (after crossing the 200 m isobath) they rapidly decelerated and moved northeastwards till they grounded north of Cape Leeuwin. This pattern is clearly seen in the buoy track between 32°30' and 34°S, in Fig. 1b; the buoy briefly reached a top speed of 1.8 m s^{-1} near the 200 m isobath.

Bernoulli's theorem states that for steady, inviscid near-surface flow, the speed q and water level h are related along a streamline by

$$\frac{q^2}{2} + gh = \text{constant}. \qquad (4)$$

The satellite-tracked buoys were drogued at 20 m and so they probably follow near-surface streamlines rather accurately. If the theorem applies, then mean sea level should fall by about 0.15 m along the buoy track, when the buoy accelerates from 0 to 1.8 m s^{-1}. If the "depth of no motion" assumptions is also valid, steric sea level should fall by about this much along the buoy track. If friction is important, the steric height fall should be greater than 0.15 m. The steric heights shown in Fig. 1b indicate a fall of order 0.15 m along the buoy track from its start near zero speed at (32°30'S, 114°20'E) to its top speed near the 200 m isobath, at 33°20'S, but it should be noted that the steric heights were obtained nearly a month before the buoy passed through the area. Nevertheless, these results illustrate that Bernoulli lowering effects may account for a substantial fraction of the 0.3 m steric height drop along the shelf edge from Fremantle to South of Cape Leeuwin, referred to in Section 4.

The mixed layer is typically 100–150 m deep in the core of the Leeuwin Current, so it is to be expected that bottom speeds will be comparable to top speeds inshore from the 200 m contour. This may account for the rapid deceleration of the buoys once they enter water shallower than 200 m: bottom speeds of (say) 1 m s^{-1} seem reasonable, implying bottom stresses of order 1.5 Pa for reasonable drag coefficients. Such stresses are very large compared to typical wind stresses. In summary, our results suggest that frictional effects, while possibly important, may not be dominant when the buoy is accelerating southwards in the deep water offshore from the 200 m isobath; but that bottom friction probably dominates once the buoy has crossed onto the continental shelf near Cape Leeuwin.

A rather different situation was found south of Cape Leeuwin. Here the most notable feature was an extremely sharp temperature and salinity front at the shelf edge south of Cape Leeuwin; it lay at an oblique angle to the continental shelf (Fig. 1a, Fig. 10a).

The along-track geostrophic Richardson number at this front was 0.39 over a depth of 175 m. This front may be the site of substantial interfacial turbulent stresses. These stresses would tend to decelerate the rapid eastward flow above the turbulent interface, and accelerate the flow beneath it. Assuming constant pressure gradient forces, the upper-layer flow will then tend to turn offshore due to decreased Coriolis forces, while the flow below the interface is likely to bend shoreward because of increased Coriolis forces: this should result in substantial penetration of cold offshore water onto the shelf. Figures 10b and 10c, showing temperature sections at BC and DEF of Fig. 1a, suggest such a penetration; while surface temperatures remain higher than 19°C on the shelf across all three sections (Figs. 10a–10c), bottom temperatures decrease from 19° to 16°C. If there are strong onshore velocities between AB and EF, near the bottom, there must also be large upward vertical motions. These must cause the warm surface water to be lifted up, thinned out and spread laterally, some of it (according to Fig. 10c) spilling well out be-

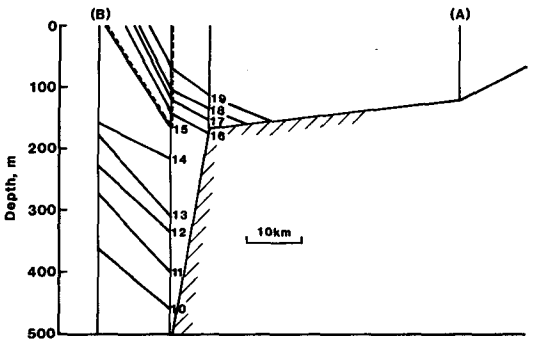

FIG. 10a. Vertical temperature section along AB of Fig. 1a. The dashed triangle surrounds a measured front; the triangle's depth and width are Δz and Δx respectively. The horizontal scale measures along-track distance.

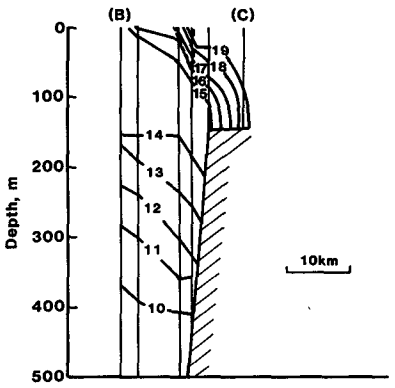

FIG. 10b. As in Fig. 10a but for the vertical temperature section along BC of Fig. 1a.

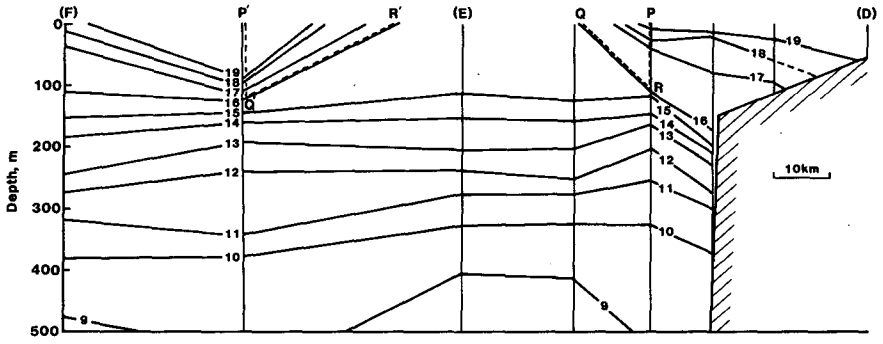

FIG. 10c. As in Fig. 10a but for the vertical temperature section along DEF of Fig. 1a. Note the course change at E.

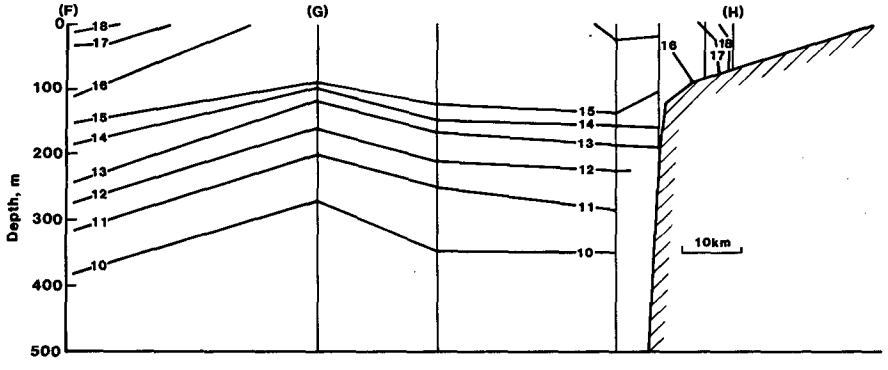

FIG. 10d. As in Fig. 10a but for the vertical temperature section along FGH of Fig. 1a. Note the course change at G.

yond the shelf. The same process will impart strong cyclonic vorticity to the water of the upper layer.

Figure 1a shows that the section across DEF, shown in Fig. 10c, intersects the warm tongue coming off the continental shelf twice—once just beyond the shelf edge, and a second time as it circles back cyclonically towards the east, crossing through EF. Figure 10c shows that the geostrophic flow associated with the tongue is rather shallow, after it has left the shelf: the 16°–19°C isotherms show strong slopes, but there is little slope to the deeper isotherms.

Figure 10d shows the vertical temperature section at FGH of Fig. 1a. The isotherms show very little downward slope as they approach the coast, i.e., the eastward geostrophic flow through this section is very small compared to that at section AB, and if 19°C

water is present over the shelf on the section at FGH, it must occur inshore of the 70 m isobath. Thus, the flux of 19°C water passing eastward through the section FGH (i.e., across 118°E) must be quite small compared to that entering the region near Cape Leeuwin: it seems that most of this water is advected offshore in the "tuft" around the cyclonic eddy centered at 116°20′E. Mixing with the underlying water may also play a role (Rochford, 1985).

The existence of offshore moving "tufts" in Fig. 1a just to the east of cyclonic eddies at 118°30′E and 122°E suggest that these eddies may play a similar role in the removal of warm water from off the continental shelf. However, our data are not adequate to be sure of this.

8. Offshore transport of saline water

Our results strongly confirm Kitani's (1977) conclusion that south of Kangaroo Island, there is a major outflow of saline water from the head of the Great Australian Bight and possibly also Spencer's Gulf: this outflow seems to be closely associated with the small, irregular anticyclonic eddy south of Kangaroo Island, seen in the buoy track of Fig. 3b.

Figure 11 shows the salinity anomaly, relative to the offshore *T–S* curve of Fig. 5, along the line XY of Fig. 3a. This was the first time on the cruise that any anomalously salty water was encountered beyond the 200 m isobath. Figure 11 is clearly compatible with Kitani's hypothesis that dense, saline water flows down the slope and pours off it, near Kangaroo Island. Quite strong temperature inversions were observed near this point, near 200 m.

The saline water apparently moves offshore; at the point Z of Fig. 3a, near the middle of the small anticyclonic eddy, a very well mixed layer was encountered that extended to 300 m below the surface. This was the only occasion on the entire cruise for which anomalously salty water was found at the surface, beyond the 200 m isobath. Its occurrence here was presumably due to vertical mixing of the salty water entering near 200 m off Kangaroo Island with the colder, fresher water above it.

This idea is further supported by the contour map of salinity at 200 m (Fig. 12). It is nearly identical in appearance to the map of steric sea level relative to 450 db (Fig. 3b). Figure 12 shows a clear separation of saline outflow regions—one south of Kangaroo Island, the second southeast of (37°40′S, 139°30′E). Both occur near locations where a shelf flow towards the southeast would be crowded seaward by a narrowing of the shelf.

The nearshore band of anomalously salty water at 200 m east of 139°30′E in Fig. 12 was associated with strong, density-compensating temperature and salinity inversions (full lines, Fig. 13). The sharply defined, homogeneous lower layer was observed at four stations close to the 200 m contour in this region. Only 10 km further offshore, however, the temperature and salinity profiles were quite different (dashed lines, Fig. 13), with no anomalously saline water present at all. The homogeneity of the saline intrusion of Fig. 13, and the sharpness of its upper boundary, suggest that this layer has only recently left the continental shelf. It is plausible that the strong northwesterly winds that developed during the preceding two days (Fig. 3b) may have created an onshore Ekman drift in the surface layers, displacing the saline shelf-water downwards and off the shelf.

9. Discussion

a. Estimation of geostrophic Richardson numbers, and stress curls from satellite images

Two particularly useful results from this cruise are that the *T–S* relationship beyond the continental shelf is quite tight along the southern Australian coast and

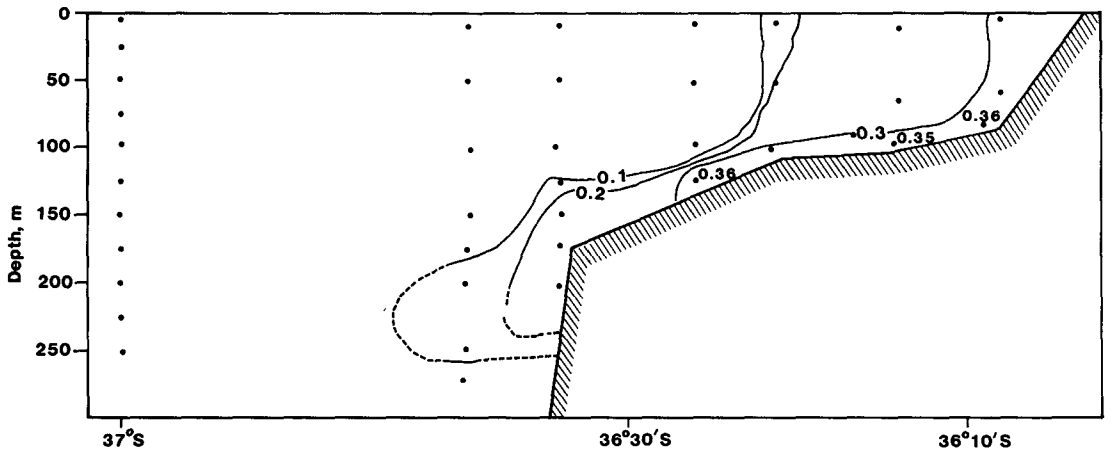

FIG. 11. The vertical salinity anomaly section, relative to the offshore *T–S* curve of Fig. 5, along the line XY of Fig. 3a.

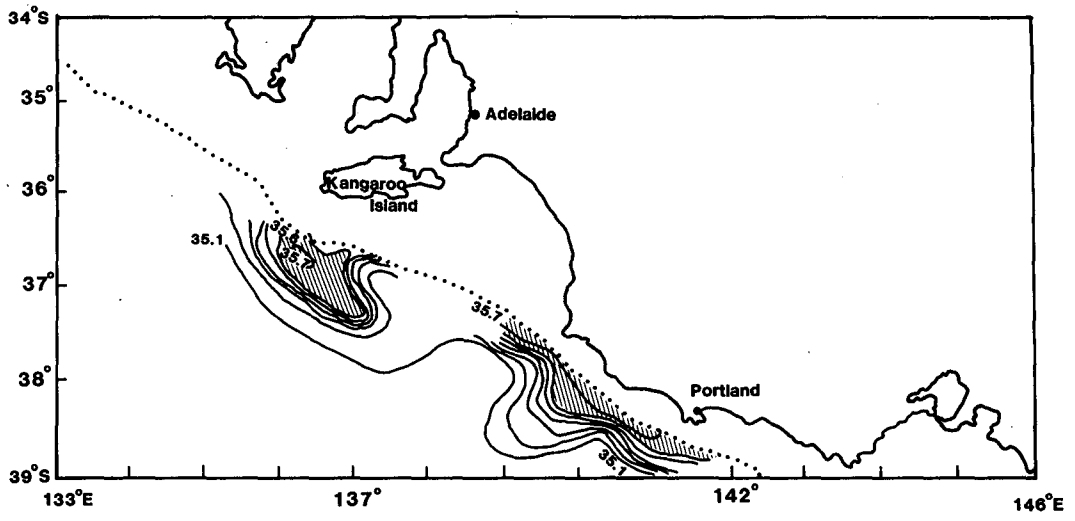

FIG. 12. Salinity isopleths at 200 m depth for 133°–146°E, 27 June–4 July 1982. In the shaded areas the salinity anomalies relative to the T–S curve of Fig. 5 are 0.1 or greater.

can be used for estimating surface densities from surface temperatures; and that for our winter cruise Δz, (the depth at which water with the surface temperature of the cold side of the front is found on the warm side) is confined in the rather narrow range 30–180 m with a peak value of about 100 m. Because of these two results, the geostrophic Richardson number can be estimated in winter from (2), within a factor of 2 or 4, from satellite images alone. Wherever $\Delta X^2/(\Delta\rho/\rho_0)$ is less than 4×10^{10} m^2, Ri_G should be of order 0.25 or less. Turbulent stresses comparable to wind stresses may occur in these regions, with very large curls.

b. *Relationships to other current systems*

Wooster and Jones (1970) found numerous laminae, 5–25 m thick in the California Undercurrent with Richardson numbers not much greater than the critical value of 0.25. McCreary (1981) concluded from these observations that vertical friction is likely to play an important role in the system; he developed a linear model containing vertical friction, which accounts quite well for the California Undercurrent and other coastal features. Our observations indicate low Richardson numbers over substantially greater depths than these; in particular we have found regions with average geostrophic Richardson number of 0.5 or less, over depths of up to 175 m (Table 1). Such conclusions must be confirmed by direct measurements of vertical velocity shear; however, at least one example of a shear layer of comparable thickness has been observed directly in the ocean. Jones (1973) found a layer 85 m deep beneath the Pacific Equatorial Undercurrent in which directly-measured Richardson numbers, averaged over 10 m depth, never exceeded 1/4. Jones estimated eddy viscosities with his data, and found that turbulent dissipation beneath the Undercurrent was large enough to account for much of the potential energy released along the path of the Undercurrent, in agreement with Wyrtki and Bennett's (1963) conclusion. Crawford (1982) has recently drawn similar conclusions.

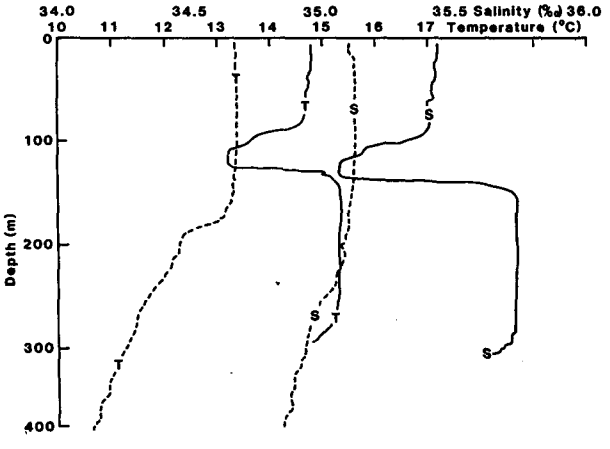

FIG. 13. Temperature (T) and Salinity (S) profiles at 38°17′S, 140°30′E (full lines) and from 10 km farther offshore (dashed lines).

Griffiths and Pearce (1985) have examined a time series of infrared satellite images of the region south of Western Australia; they conclude that the eddies in this region are very similar to "modons" observed in laboratory experiments (e.g., Flierl et al., 1983). Baroclinic instability is thought to play an important role in the formation of modons. Our results support this idea, though they also suggest that friction and diffusion may play important roles. In particular, we have suggested that the "tuft" of warm water leaving the coast near 116°30′E may have come about as a result of the

action of the interfacial stresses near the sharp front south of Cape Leeuwin.

10. Summary

Buoy tracks, ship's drift vectors and sea surface temperatures (SSTs) along Australia's south coast in June–July 1982 showed a narrow shelf-edge current flowing eastwards along the entire distance; cyclonic eddies broke away from the shelf west of 124°E, and broad anticyclonic loops were observed east of 124°E. A single well-defined T–S relationship was satisfied at stations beyond the 1000 m isobath; west of 124°E, it applied quite well also on the continental shelf, but from 124°E to 135°E positive salinity anomalies became progressively larger on the shelf. This saline water was not observed beyond the shelf anywhere west of 135°E, but a strong jet of it appeared to flow off the shelf west of Kangaroo Island; the small anticyclonic eddy found south of Kangaroo Island contained anomalously saline water at its core, in a surface mixed layer extending to 300 m depth. A second region of well-defined offshelf flow of anomalously saline water and marked temperature inversions occurred just offshore from the region of narrow continental shelf between 139°E and 142°E.

Forty-five surface temperature fronts were crossed during the voyage. Along track geostrophic Richardson numbers were measured on 34 of them; of these 34 values, four were less than 0.25 and ten were less than 1.0, suggesting that Kelvin–Helmholtz instability and turbulent interfacial stresses may occur frequently in these fronts. Further sharp fronts in salinity alone occurred over the continental shelf. A particularly strong front was observed near the continental shelf edge, south of Cape Leeuwin. It is postulated that strong interfacial stresses occur across this front, and that these are at least in part responsible for the fact that after they round Cape Leeuwin, the warm Leeuwin Current waters become shallower and broader, and spin out to sea in one or more cyclonic eddies. This eddying process seems to remove most of the warmest water from off the continental shelf.

Steric sea level relative to 450 db near the 500 m isobath fell about 0.3 m from Fremantle to Albany, around Cape Leeuwin, a distance of 400 km. Bottom stresses or interfacial stresses that are large compared to typical wind stresses of 0.1 Pa are required to balance these strong longshelf pressure gradients: our results suggest that such strong stresses occur near Cape Leeuwin. The Bernoulli effect may also play a role locally in balancing the longshelf pressure gradient: one satellite-tracked buoy accelerated from zero to 1.8 m s^{-1} in 100 km, implying a sea level lowering of about 0.15 m by Bernoulli's theorem.

A side result of our work is the finding that in winter, geostrophic Richardson numbers at shelf-edge fronts may be crudely estimated from satellite infrared images alone.

Acknowledgments. The success of this cruise was in large measure due to George Cavill and Ralph Masterson, the master and mate of R/V *Sprightly*. George has the disconcerting habit of telling one about important scientific events (crossing fronts, etc.) before one has noticed them on one's instruments: he feels them. He has recently retired, and he will be sorely missed. Alan Pearce's work on WAIT satellite photographs is much appreciated. Messrs. G. Wilkins, R. Schahinger, A. Poole, R. Griffiths, A. Knight and M. Nelson all shared the labors of this cruise, and the comments of George Cresswell and Eric Lindstrom have been helpful in preparing this paper.

REFERENCES

Crawford, W. R., 1982: Pacific equatorial turbulence. *J. Phys. Oceanogr.*, **12,** 1137–1149.

Cresswell, G. R., and D. J. Vaudrey, 1977: Satellite-tracked buoy data report I: Western Australian releases 1975 and 1976. CSIRO Div. of Fisheries and Oceanography Rep. No. 86.

——, and T. J. Golding, 1980: Observations of a south-flowing current in the south-eastern Indian Ocean. *Deep-Sea Res.*, **27A,** 449–466.

Flierl, G. R., M. E. Stern and J. A. Whitehead, Jr., 1983: The physical significance of modons: laboratory experiments and general integral constraints. *Dyn. Atmos. Oceans,* **7,** 233–264.

Godfrey, J. S., and K. R. Ridgway, 1985: The large scale environment of the poleward-flowing Leeuwin Current, Western Australia: Longshore steric height gradients, wind stress and geostrophic flow. *J. Phys. Oceanogr.*, **15,** 481–495.

——, G. R. Cresswell and F. M. Boland, 1980: Observations of low Richardson numbers and undercurrents near a front in the East Australian Current. *J. Phys. Oceanogr.*, **10,** 301–307.

Griffiths, R., and A. F. Pearce, 1985: Instability and eddy pairs on the Leeuwin Current South of Australia. Submitted to *Deep-Sea Res.*

Jones, J. H., 1973: Vertical mixing in the Equatorial Undercurrent. *J. Phys. Oceanogr.*, **3,** 286–296.

Kitani, K., 1977: Some observations on the temperature inversion south of Kangaroo Island, southern Australia. *Bull, Far Seas Fish. Res. Lab.*, **15,** 1–11.

Legeckis, R., and G. R. Cresswell, 1981: Satellite observations of sea-surface temperature fronts off the coast of western and southern Australia. *Deep-Sea Res.*, **28A,** 297–306.

McCreary, J., 1981: A linear stratified ocean model of the coastal undercurrent. *Phil. Trans. Roy. Soc. London,* **A302,** 385–413.

Provis, D. G., and G. W. Lennon, 1981: Some Oceanographic Measurements in the Great Australian Bight. *Proc. Fifth Australian Conf. on Coastal and Ocean Engineering,* Perth, The Institution of Engineers.

Ridgway, K. R., and R. G. Loch, 1985: Mean T–S Relationships and their Application in Computing Dynamic Height from Temperature Profiles around Australia. *Aust. J. Mar. Freshwater Res.*, (in press).

Rochford, D. J., 1985: The eastward limit of the Leeuwin Current. *Aust. J. Mar. Freshwater Res.* (in press).

Thompson, R. O. R. Y., 1984: Observations of the Leeuwin Current off Western Australia. *J. Phys. Oceanogr.*, **14,** 623–628.

Turner, J. S., 1973: *Buoyancy Effects in Fluids.* Cambridge University Press, 367 pp.

Wooster, W. S., and J. H. Jones, 1970: California Undercurrent off Baja California. *J. Mar. Res.*, **28,** 235–250.

Wyrtki, K., and G. D. Bennett, 1963: Vertical eddy viscosity in the Pacific Equatorial Undercurrent. *Deep-Sea Res.*, **10,** 449–455.